

pubs.acs.org/jpr Article

# Improved Method to Determine Protein Turnover Rates with Heavy Water Labeling by Mass Isotopomer Ratio Selection

Published as part of Journal of Proteome Research Special Issue "Software Tools and Resources 2025".

Jordan Currie, Dominic C. M. Ng, Boomathi Pandi, Alexander Black, Vyshnavi Manda, Cheyanne Durham, Jay Pavelka, Maggie P. Y. Lam, and Edward Lau\*



Cite This: https://doi.org/10.1021/acs.jproteome.4c01012



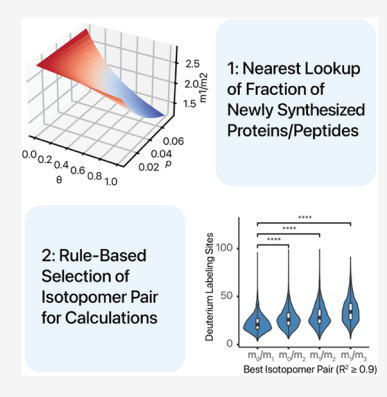
**ACCESS** 

III Metrics & More

Article Recommendations

Supporting Information

**ABSTRACT:** The synthesis and degradation rates of proteins form an essential component of gene expression control. Heavy water labeling has been used in conjunction with mass spectrometry to measure protein turnover rates, but the optimal analytical approaches to derive turnover rates from the mass isotopomer patterns of deuterium-labeled peptides continue to be a subject of research. Here, we describe a method that comprises (1) a nearest lookup of numerically approximated peptide isotope envelopes, coupled to (2) the selection of optimal mass isotopomer pairs based on peptide sequence rules, to calculate the molar fraction of new peptide synthesis in heavy water labeling mass spectrometry experiments. We validated our approach using an experimental calibration standard comprising mixtures of fully unlabeled and fully labeled proteomes. We then reanalyzed 17 proteome-wide turnover experiments from four mouse organs across multiple data sets and showed that the combined nearest-lookup and rule-based mass isotopomer ratio selection method increases the coverage of well-fitted peptides in protein turnover experiments by up to  $58 \pm 13\%$ . The workflow is implemented in the Riana



software tool for protein turnover analysis and may avail ongoing efforts to study the synthesis and degradation kinetics of proteins in animals on a proteome-wide scale.

KEYWORDS: mass spectrometry, protein turnover, heavy water, deuterium, mass isotopomer, software

#### INTRODUCTION

It is not possible to discern the relative contributions of synthesis and degradation to changes in protein concentration. Turnover (the combined processes of synthesis and degradation) continues, for nearly all proteins, in the absence of any change in the protein level, the "steady state". Accordingly, the only way to assess turnover parameters is by monitoring the flux of a label (whether stable or less commonly now, unstable, radioactive isotopes) through the protein pool. Stable isotope labeling can employ amino acids or simple metabolic precursors, such as heavy water or [<sup>15</sup>N]-labeled ammonium ions.

Heavy water labeling, coupled with mass spectrometry, can be used to trace the synthesis and degradation kinetics of proteins in rodents and in humans.  $^{1-13}$  Under continued enrichment of heavy water  $D_2O$ , deuterium (D or  $^2H$ ) atoms are incorporated into nonessential amino acids during biosynthesis and metabolism. The deuterium-labeled amino acids are in turn incorporated into nascent protein chains. The isotope incorporation rate over time reflects the rate of turnover of the protein pool. Water labeling is not readily compared with other forms of amino acid labeling, in which tracer amino acids are labeled consistently with a fixed number of  $^{13}C$  or  $^{15}N$  atom centers. These give a fixed mass offset per amino acid instance that is the same irrespective of the amino acid sequence,

exemplified by SILAC or dynamic SILAC approaches. By contrast, heavy water labeling varies from one amino acid to another and thus, the degree of labeling of a peptide is sequencedependent. Moreover, while <sup>13</sup>C or <sup>15</sup>N amino acid labeling can be initiated with 100% of the amino acid pool being labeled, this is not feasible with water labeling; enrichment of 10% or less excess deuterium is usual. The combination of partial labeling and the variable number of labeled atom centers in each amino acid means that peptides exhibit complex labeling patterns, showing a gradual trajectory of increasing and overlapping mass without clear isotope separation typified by SILAC. The SILAC fixed mass offset greatly simplifies downstream data analysis, particularly as the labeled mass offset can mean that there is negligible contamination of the labeled mass isotopomer distribution with the unlabeled mass isotopomer distribution. With heavy water labeling, the mass isotopomer profile gradually shifts from unlabeled to labeled with considerable overlap of

Received: November 13, 2024 Revised: March 2, 2025 Accepted: March 5, 2025



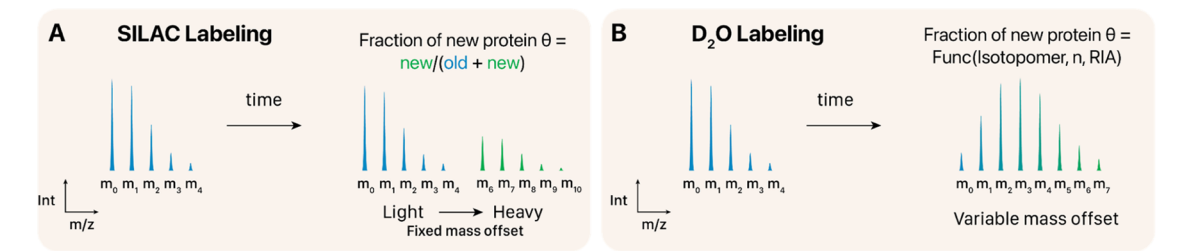


Figure 1. Data analysis in  $D_2O$  labeling. Comparison of (A) SILAC and (B) heavy water labeling. SILAC labeling leads to fixed mass offset. The full replacement of the labeled residue with the heavy version with multiple heavy atom centers lends to relatively easy calculation of the molar fraction of newly synthesized proteins  $\theta$ . Water labeling on the other hand is performed at low ( $\leq$ 10%) precursor isotope enrichment and moreover leads to gradual shifts in the isotope envelope that are highly dependent on peptide sequences.

labeled and unlabeled profiles, leading to complex isotopic patterns (Figure 1A).

A critical step of the data analysis is to calculate the molar fraction of newly synthesized proteins,  $0 \le \theta \le 1$ , from the peptide isotope envelope of an MS1 spectrum. Commonly, this measurement is performed by considering the ratio of the monoisotopomer (i.e., the first mass isotopomer,  $m_0$ ) over the complete isotope profile of the peptide  $m_0/\sum m_i$ . The complete profile is typically computed from the intensities of the first six mass isotopomers ( $m_0$ : $m_5$ ) (Figure 1B). However, it should be noted that for longer peptides and depending on the enrichment level,  $m_6$  and higher mass isotopomer peaks can also be expected to be present in appreciable proportions. For instance, a peptide with 26 averagine residues will have 1% relative abundance in the  $m_6$  mass isotopomer prior to labeling, which increases to 10.1% assuming a conservative one label-accessible hydrogen atom per residue at 4.6% background deuterium enrichment.

Because of the gradual shift in the mass isotopomer profile, the ratio of any pair of mass isotopomers contains information about the degree of deuterium enrichment. Partial mass isotopomer profiles (such as from a pair of mass isotopomers) could, in principle, be sufficient for calculating the fraction of newly synthesized proteins. Recently, Sadygov and colleagues derived closed-form analytical formulas for calculating the abundance ratios of the  $m_1-m_5$  mass isotopomers as a function of deuterium enrichment and amino acid labeling sites. These formulas permitted calculation of the most probable deuterium enrichment from the corresponding mass isotopomer ratio, from which the relative abundance of the monoisotopomer and turnover rates is calculated. <sup>14</sup> The use of partial mass isotopomer ratios (e.g.,  $m_0/m_1$ ) gave increased performance over using the full isotope envelope, as measured by the number of peptides whose mass isotopomer time series can be fitted well to a kinetic model (with  $R^2 \ge 0.9$ ). The authors suggest that this is due to the reduced chance of interfering with isobaric contaminants in the isotopic cluster when only two mass isotopomer peaks need to be quantified. However, a limitation is that each mass isotopomer ratio calculation requires a separate combinatorics calculation, and not all formulas ( $m_6$  and beyond) are demonstrated.

As an alternative, the individual mass isotopomer profiles of a peptide can also be calculated numerically with an isotope fine structure calculation algorithm such as  $IsoSpec2^{15}$  and enviPat, <sup>16</sup> which considers all isotopologue combinations of a compound given its chemical composition. The isotope envelope of a labeled peptide can be simulated by using the isotope fine structure calculator with a custom elementary composition table, which can resolve the probability (i.e., proportional abundance) of mass isotopomers beyond  $m_5$ . In

this study, we describe a workflow to analyze heavy water labeling mass spectrometry data with two components. (1) Numerical Lookup of Nearest  $\theta$ : First, we show that the calculated isotopologue probability method can be applicable to heavy water-based protein turnover analysis and allows any arbitrary combination of mass isotopomer profiles to be directly queried numerically (e.g.,  $m_1/m_3$ ,  $m_1/(m_0+m_1+m_2)$ ,  $m_0/m_1$  $\sum (m_0:m_8)$ , etc.) without requiring the closed-form analytical solutions. A numerical lookup is then used to compare empirical mass isotopomer pair ratios to mixture spectra to find the  $\theta$  value of a sampled peptide. This is termed the "Nearest-Lookup" method in the manuscript. (2) Rule-based Mass Isotopomer Ratio Selection: We next analyzed which of the mass isotopomer pairs within the peptide isotope envelope yielded mass isotopomer time courses that fit most closely to kinetic models and found that the identity of the best pair of mass isotopomers to use depends partially on the number of deuterium-accessible labeling sites of the peptide. We derived a strategy to select the mass isotopomer ratios to calculate turnover rates based on predefined rules of parameters calculated from the peptide sequence, referred to as the "Rule-Based Selection" method in the manuscript. Combined, the two methods increase the coverage of existing proteome-wide turnover experiments in multiple data sets of the mouse heart, liver, kidney, and skeletal muscle over the "Conventional Method" of calculating  $m_0/\sum m_i$  by up to  $58 \pm 13\%$ .

#### METHODS

#### **Cell Culture and Mass Spectrometry**

For calibration samples, human AC16 cells (Millipore) were cultured in DMEM/F12 supplemented with 10% fetal bovine serum (FBS) and either 6% D<sub>2</sub>O (heavy labeled population) or 6% H<sub>2</sub>O (control population) at 37 °C, 5% CO<sub>2</sub>. The cells were maintained in this medium for 3 passages, each passage with a split ratio of 1:8. This growth was estimated to constitute approximately 9 doublings of the cell populations. The cells were harvested by trypsinization, pelleted, washed once with phosphate buffered saline, and pelleted again before snapfreezing in liquid nitrogen and storing at −80 °C. At the time of processing, each pellet was resuspended in 1 mL of RIPA buffer (Thermo Scientific) supplemented with Halt Protease and Phosphatase Inhibitor Cocktail (Thermo Scientific). Proteins were extracted with sonication in a Bioruptor Pico (Diagenode) with settings 10× 30 s on 30 s off at 4 °C. Insoluble debris was pelleted and removed from all samples by centrifugation at 14,000g, 5 min.

Protein concentration of all samples was measured with Rapid Gold BCA (Pierce). Cell lysates from the  $D_2O$  and  $H_2O$  media

populations were then combined in a labeling series expressed as the proportion of protein that was labeled with heavy water: 0, 0.125, 0.25, 0.375, 0.5, 0.625, 0.75, 0.875, and 1. The samples were trypsin-digested using a modified version of the filter-aided sample preparation approach as previously described. A total of 50  $\mu$ g of protein per sample in 250  $\mu$ L of 8 M urea was loaded onto Pierce Protein Concentrators PES, 10K MWCO (Thermo Scientific) prewashed with 100 mM ammonium bicarbonate (Ambic). The samples were again washed with 8 M urea to denature proteins and remove sodium dodecyl sulfate (SDS). The samples were washed with 300  $\mu$ L of 100 mM Ambic twice. The samples were then reduced and alkylated with final concentrations of 5 mM dithiothreitol (DTT) and 18 mM iodoacetamide (IAA) for 30 min at 37 °C in the dark. DTT and IAA were removed with centrifugation, and the samples were washed  $3\times$  with 100 mM Ambic. Samples were digested atop the filters overnight at 37 °C with mass spectrometry-grade trypsin (Promega) at a ratio of 1:50 enzyme:protein. The following day, the samples were cleaned with Pierce C18 spin columns (Thermo Scientific) according to the manufacturer's protocol. The eluted peptides were dried under vacuum and redissolved and resuspended in 0.1% (v/v) formic acid.

The samples were analyzed on a Thermo Q-Exactive HF quadrupole-Orbitrap mass spectrometer coupled to a nanoflow Easy-nLC UPLC instrument with the Thermo EasySpray electrospray ionization source. Peptides were separated with a PepMap RSLC C18 column 75  $\mu$ m × 15 cm, 3  $\mu$ m particle size (Thermo Scientific) with a 90 min gradient from 0 to 100% pH 2 solvent B (0.1% formic acid in 80% v/v LC-MS-grade acetonitrile). The mass spectrometer was operated in datadependent acquisition mode with scans between m/z 200 and 1650 acquired at a mass resolution of 60,000. The maximum injection time was 20 ms, and the automatic gain control (AGC) was set to 3e6. MS2 scans of the 15 most intense precursor ions with charge states of 2+ to 5+ were acquired with an isolation window of 2 m/z units, maximum injection time of 110 ms, and automatic gain control of 2e5. Fragmentation of the peptides was by a stepped normalized collision-induced dissociation energy (NCE) of 25–27. Dynamic exclusion of m/z values was used with an exclusion time of 30 s.

#### Calculation of the Fraction of Newly Synthesized Proteins

The determination of the protein turnover rate through heavy water labeling requires interpretation of the pattern of isotope incorporation in heavy water labeled peptides to recover the fraction of newly synthesized proteins as a function of the period of labeling. Isotope incorporation is commonly traced using the change in  $m_0$  (i.e., monoisotopomer)/ $\sum m_i$  (i.e., the complete isotope profile) over labeling points.  $\sum m_i$  is typically only quantified for the first six mass isotopomers (i.e., i = 0 to 5). <sup>2,8,18</sup> For the  $m_0/\sum m_i$  calculation (also referred to as  $A_0$  or  $m_0/m_A$  for m "all" below), as the protein pool turns over, the mass isotopomer profile is assumed to traverse linearly from the initial position, i.e., the theoretical natural distribution of experimentally unlabeled peptides, calculated from the biosphere abundance of isotopes of C, H, O, N, and S, toward the final asymptotic distribution that is determined by the precursor isotope abundance and number of accessible labeling sites of the peptides. The initial coordinate of  $m_0/\sum m$ , or  $A_0(0)$ , can be calculated given the absence (other than natural abundance) of heavy isotopes in any of the atoms in the peptide, using eq 1. The fully labeled asymptote, often not achieved in a labeling experiment, is modeled on the initial (prelabeling) isotopomer

profile, conditioned by complete incorporation of amino acids in which the deuterium abundance is as high as can be achieved given the water enrichment with deuterium

$$A_0(0) = \prod_{\text{ele}} (p_{\text{ele}}^{n_{\text{ele}}}); \text{ ele} \in [C, H, O, N, S]$$
 (1)

The plateau of  $A_0$  is calculated as the product of naturally occurring  $A_0$ , multiplied by the probability of a molecule not having any of the enriched labels on any atom. The latter is a function of the number of deuterium-accessible stable labeling sites on the peptide  $n_b$  and p, the precursor relative isotope abundance, i.e., the atomic percent of deuterium introduced in water in the experiment (eq 2)

$$A_0^{\text{asymp}} = A_0(0) \cdot (1 - p)^{n_l} \tag{2}$$

The use of *p* can be refined by considering naturally occurring deuterium to calculate the atomic percent excess over background deuterium, but the background deuterium level is negligible and may be ignored.

It can be seen that the number of deuterium exchangeable sites  $n_l$  is a critical variable for the interpretation of labeling data. The value of  $n_l$  for the limited set of peptides measured in the calibration standard samples can be calculated directly from eq 2, as the plateau value of  $A_0$  is experimentally determined. In a large-scale labeling experiment where peptides cannot be assumed to have plateaued,  $n_l$  for any peptide can be calculated from the amino acid composition of the peptide and the individual amino acid labeling sites

$$n_l = \sum n_a \cdot N_a \tag{3}$$

The individual amino acid labeling sites are calculated using literature values from Commerford et al. <sup>19</sup> (Table 1).

Table 1. Number of Label-Accessible Hydrogen Atoms per Amino Acid Residue in Animal Labeling Experiments Used in the Analysis of This Study $^a$ 

amino acid	exchangeable H atoms	amino acid	exchangeable H atoms
A	4.00	M	1.12
C	1.62	N	1.89
D	1.89	P	2.59
E	3.95	Q	3.95
F	0.32	R	3.34
G	2.06	S	2.61
Н	2.88	T	0.2
I	1.00	V	0.56
K	0.54	W	0.08
L	0.69	Y	0.42

<sup>&</sup>lt;sup>a</sup>The values were measured from tritium labeling in adult mice in Commerford et al. <sup>19</sup>

During a dynamic labeling experiment,  $A_0$  changes as a function of time as new proteins are synthesized and existing proteins are degraded

$$A_0(t) = m_{i=0}(t) / \sum_{i=0}^{5} m_i(t)$$
(4)

The fraction of newly synthesized proteins/peptides  $\theta$  at a given time t is therefore calculated from  $A_0(t)$  as

$$\theta = (A_0(t) - A_0(0))/(A_0^{\text{asymp}} - A_0(0))$$
(5)

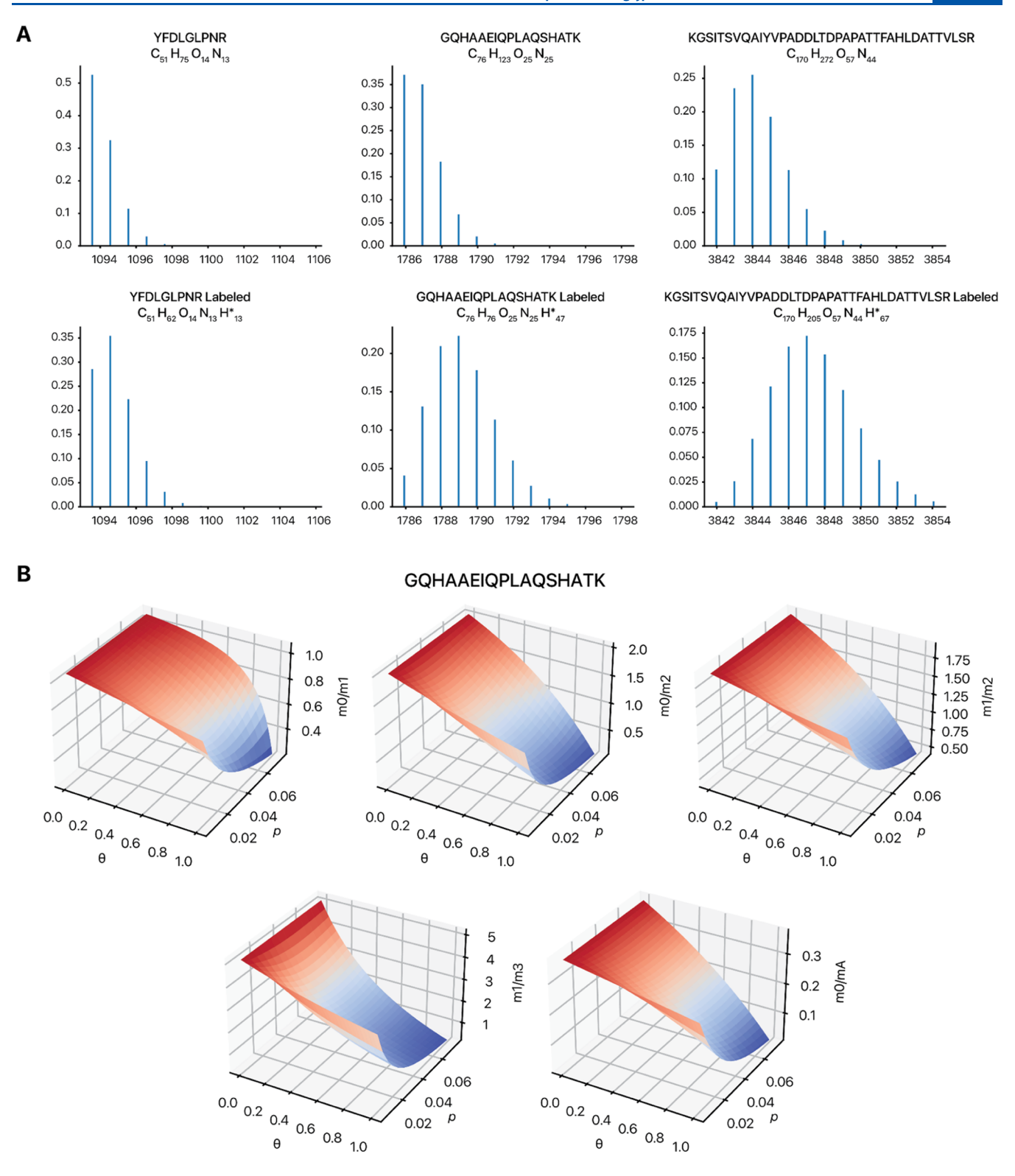


**Figure 2.** Simulated isotope envelopes in heavy water labeled samples. (A) Simulated spectra showing the calculated isotopic envelopes based on element count and custom element count for three peptides that have been empirically quantified in a prior heavy water labeling data set (Hammond et al.). (Left) A shorter peptide with few deuterium label sites, a medium-length peptide with a relatively high number of heavy water labeling sites, and a long peptide with many deuterium labeling sites. For each peptide, the top plot represents the simulated naturally occurring isotope envelope (prelabeling), and the bottom plot represents the asymptotic isotope envelope following labeling with 4.6% relative isotope abundance (p) of heavy water. Appreciable  $m_6$  peaks can be seen in the long peptide prior to labeling and medium and long peptides after labeling. (B) Contour plots showing the relationship between the fraction of newly synthesized proteins/peptides ( $\theta$ ), heavy water enrichment (p), and the mass isotopomer ratio of different measurements, including  $m_0/m_1$ ,  $m_0/m_2$ ,  $m_1/m_2$ ,  $m_1/m_3$ , and  $m_0/m_A$ . Within each experimental p value under the shown range (x-axis),  $\theta$  maps one-to-one to the shown ratios but with different spans.

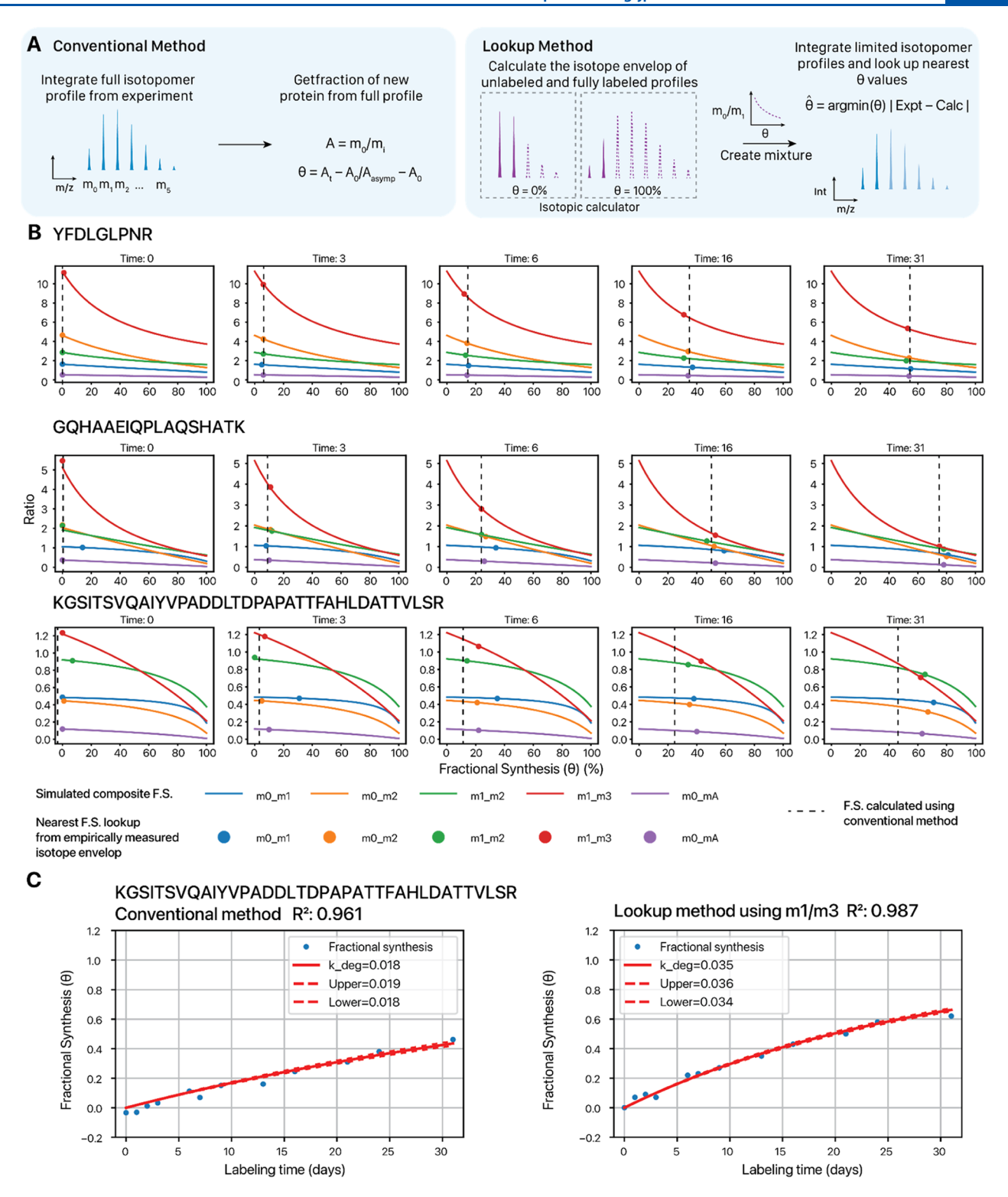


Figure 3. Estimating the fraction of newly synthesized proteins/peptides from simulated composite spectra. (A) (Left) Conventional method to calculate the molar fraction of new proteins from isotopic profiles traces the fractional abundance of the first mass isotopomer ( $m_0$ ) without any heavy atom center over the entire isotope envelope. However, this method requires integration over many mass isotopomers and is prone to isobaric contamination or loss of the  $m_0$  signal in long peptides. (Right) The nearest-lookup method uses a fine structure isotopic calculator to predict the isotope envelope for an unlabeled peptide ( $\theta = 0$ ) as well as a fully turned over labeled peptide ( $\theta = 1$ ). The virtual isotope envelopes are then mixed at different proportions to trace the relationship of any isotopic pairs with  $\theta$ . This curve is then used to look up  $\theta$  from the limited isotopic profiles (e.g.,  $m_0/m_2$  or  $m_0/m_1$ ) from the experimental data. (B) Lines show the values of different mass isotopomer ratios (colors) in simulated composite spectra mixed from 0 to 100% unlabeled and asymptotic peptide isotope envelopes. The data point shows the nearest estimated  $\theta$  from experimental data for the three peptides in consideration; from Hammond et al. The black dashed line shows the  $\theta$  value for the peptide at each time point as calculated using conventional methods in the original publication. (C) Kinetic curve fitting of the peptide KGSITSVQAIYVPADDLTDPAPATTFAHLDATTVLSR with  $\theta$  values calculated from the conventional method (left) and the  $m_1/m_3$  mass isotopomer ratio (right).

The intensity of the  $m_1$  isotopomer can be derived by a closed-form equation as a function of excess deuterium enrichment. The intensities of the asymptotic abundance ratios up to the first six mass isotopomers  $(m_1, m_2, m_3, m_4, \text{ and } m_5)$  were reported by Sadygov and colleagues. <sup>14</sup>

As an alternative to closed-form equations for peptide mass isotopomers, isotopic fine structure calculation algorithms can be used to resolve the isotopologues of any compound prior to and after deuterium labeling. Here, we used IsoSpecR and IsoSpecPy, which provide bindings to the IsoSpec2<sup>15</sup> algorithm in R and Python, respectively, to estimate the probability of isotopic combinations based on an elemental isotopic composition table. The heavier isotopes in peptides are largely driven by <sup>15</sup>N and <sup>13</sup>C; an isotope abundance of 0.003642 is used for <sup>15</sup>N and 0.010788 is used for <sup>13</sup>C in IsoSpecR. The <sup>13</sup>C abundance is consistent with NIST values and corresponds to a  $\delta^{13}$ C of approximately -17 per VPDB standard ( $^{13}$ C/ $^{12}$ C of 0.011100), which is typical for biological materials. The isotopologue probabilities are then summed into mass isotopomers.

The prelabeling and asymptotic predicted spectra are then summed into a series of composite spectra of any proportion of labeled and unlabeled peptides. These composite spectra are then compared to an experimental spectrum to estimate the fraction of newly synthesized peptide  $\theta$  from the mass isotopomer pairs of a peptide envelope

$$\begin{split} \hat{\theta_t} &= arg\min(\theta) |R_{\text{exp}t}(t) - (R_{\text{calc}}(0) \cdot (1-\theta) + R_{\text{calc}}^{\text{asymp}}(\theta))| \\ &; \ 0 \leq \theta \leq 1 \end{split} \tag{6}$$

where *R* is an applicable mass isotopomer ratio calculation, e.g.,  $m_0/m_1$ ,  $m_0/\sum (m_0:m_5)$ , etc.

#### **Kinetic Modeling and Statistical Analysis**

Mass spectrometry data for the calibration standard and for PXD029639 were searched against UniProt Swiss-Prot database retrieved using Philosopher v.4.8.1 on 2023-06-27 with added contaminants using Comet v.2022.01 with typical parameters including: decoy\_search = 1; peptide\_mass\_tolerance: 10.00 ppm; num\_enzyme\_termini = 1; isotope error: 0/1/2/3; fragment\_bin\_tol = 0.02; fragment\_bin\_offset = 0.0. Search results were postprocessed using Percolator (crux-4.1 distribution) with the following options: --decoy-prefix DECOY\_; --overwrite T; --maxiter 15; --picked-protein. A peptide identification at an FDR adjusted q value of 0.01 is considered a confident identification. For the FT/IT data in PXD002870 and PXD036140, low-resolution MS2 settings were used including fragment\_bin\_tol = 1.0005 and fragment\_bin offset = 0.4.

Mass isotopomer intensity was extracted using Riana v.0.8.0° to extract the intensity over time of the  $m_0$ ,  $m_1$ ,  $m_2$ ,  $m_3$ ,  $m_4$ , and  $m_5$  peaks. The fraction of newly synthesized proteins/peptides  $\theta$  was calculated as detailed above. The time series of  $\theta$  at different experimental time points was then fitted to a kinetic model to obtain the best-fit turnover rate constant ( $k_{\rm deg}$ ) to explain the time series. For the reanalyzed adult mouse  $in\ vivo\$ data, to perform kinetic modeling, we used the two-compartment model as described in Guan et al.  $^{24}$  to find the best-fit  $k_{\rm deg}$ , with a high precursor equilibration rate constant ( $k_{\rm p} = 3.0\ {\rm d}^{-1}$ ) that reflects the fast equilibration of heavy water with the protein precursor pool  $^{6,9}$  and the steady-state precursor isotope enrichment ( $p_{\rm ss}$ ) as reported in the original studies.

#### RESULTS

#### Determination of the Fraction of Newly Synthesized Proteins in Heavy Water Labeling Experiments Using an Isotopic Calculation Algorithm

Using the isotopic fine structure calculation algorithm IsoSpec2, the asymptote isotope envelope of a peptide can be resolved by including an artificial element (H\*) that represents the number of label-accessible hydrogen atoms in the sequence with a probability of deuterium mass (2.0141 u) equal to the background enrichment level of heavy water in the experiment, which can be determined from direct measurement of body fluid by GC-MS or by direct fitting from peptide experimental data.<sup>6</sup> A heavy water enrichment of 4.6% as from the mouse experiments in Hammond et al.<sup>6</sup> is used in the analysis here. The number of H\* atoms is then subtracted from the total number of hydrogen atoms. Figure 2A shows the simulated naturally occurring (prelabeling) isotope envelope and asymptotic labeled envelope for three peptides: a relatively short peptide with few deuterium label sites (YFDLGLPNR from mitochondrial isocitrate dehydrogenase, MW 1093.56, number of deuterium-accessible labeling site  $n_l \sim 13$ ; essential amino acids underlined); a medium-length peptide with many nonessential amino acids and thus heavy water labeling sites (GQHAAEIQPLAQSHATK from myoglobin, MW 1785.91, n<sub>l</sub>  $\sim$  47), and a very long peptide with many deuterium labeling sites (<u>K</u>GS<u>ITSV</u>QA<u>I</u>Y<u>V</u>PADD<u>LT</u>DPAPA<u>TTF</u>A<u>HL-</u> DATTVLSR from ATP synthase subunit  $\beta$ , MW: 3841.97, n<sub>l</sub>  $\sim$  67). In the two longer peptides, particularly at asymptotic (4.6%) deuterium enrichment, there are appreciable m<sub>6</sub> and higher probabilities present, which would indicate that the typical  $m_0/\sum (m_0:m_5)$  calculation underestimates isotope incorporation (Figure 2A). This may be mitigated by expanding the conventional  $m_0/\sum m_i$  method to include for example integrating over up to the 10th mass isotopomer  $(m_0:m_0)$  for peptides with more predicted labeling sites. However, integration over multiple signal peaks leads to higher chances of contaminant isobaric peptides interfering with the quantification. The isotopic envelopes of user-input peptide sequences can be visualized on a web app at http://heart.shinyapps.io/ D2O Isotope/.

Three-dimensional contour plots for the same three peptides in Figure 2A are shown in Figures 2B and S1. The contours show the change of multiple mass isotopomer ratios as a function of the fraction of newly synthesized proteins/peptides  $\theta$  and the common range of heavy water labeling used in experiments (1–8%):  $m_0/m_1$ ,  $m_0/m_2$ ,  $m_1/m_2$ ,  $m_1/m_3$ , and  $m_0/m_A$  (i.e.,  $\sum (m_0:m_5)$ ), confirming that the ratios of each pair map to unique functional synthesis values given a particular known experimental precursor isotope enrichment. It can further be seen that the span and sensitivity of the mass isotopomer ratio vs  $\theta$  relationship also depends on the background isotope enrichment (e.g., % deuterium in the system; p in the graphs below) and peptide sequence (number of labeling sites).

We then simulated the composite spectra by mixing linearly different proportions of the prelabel and postlabel spectra (Figure 3A). In this way, the empirically quantified ratios from any mass isotopomer pairs in an experiment (e.g., the intensity of the  $m_0$  peak divided by the  $m_1$  peak in the experiment) can be used to find the value of  $\theta$  that would lead to the composite spectrum in eq 6 that best matches empirical values. To evaluate how well the simulated composite spectra can be used to derive  $\theta$  from the empirically measured isotope envelope, we

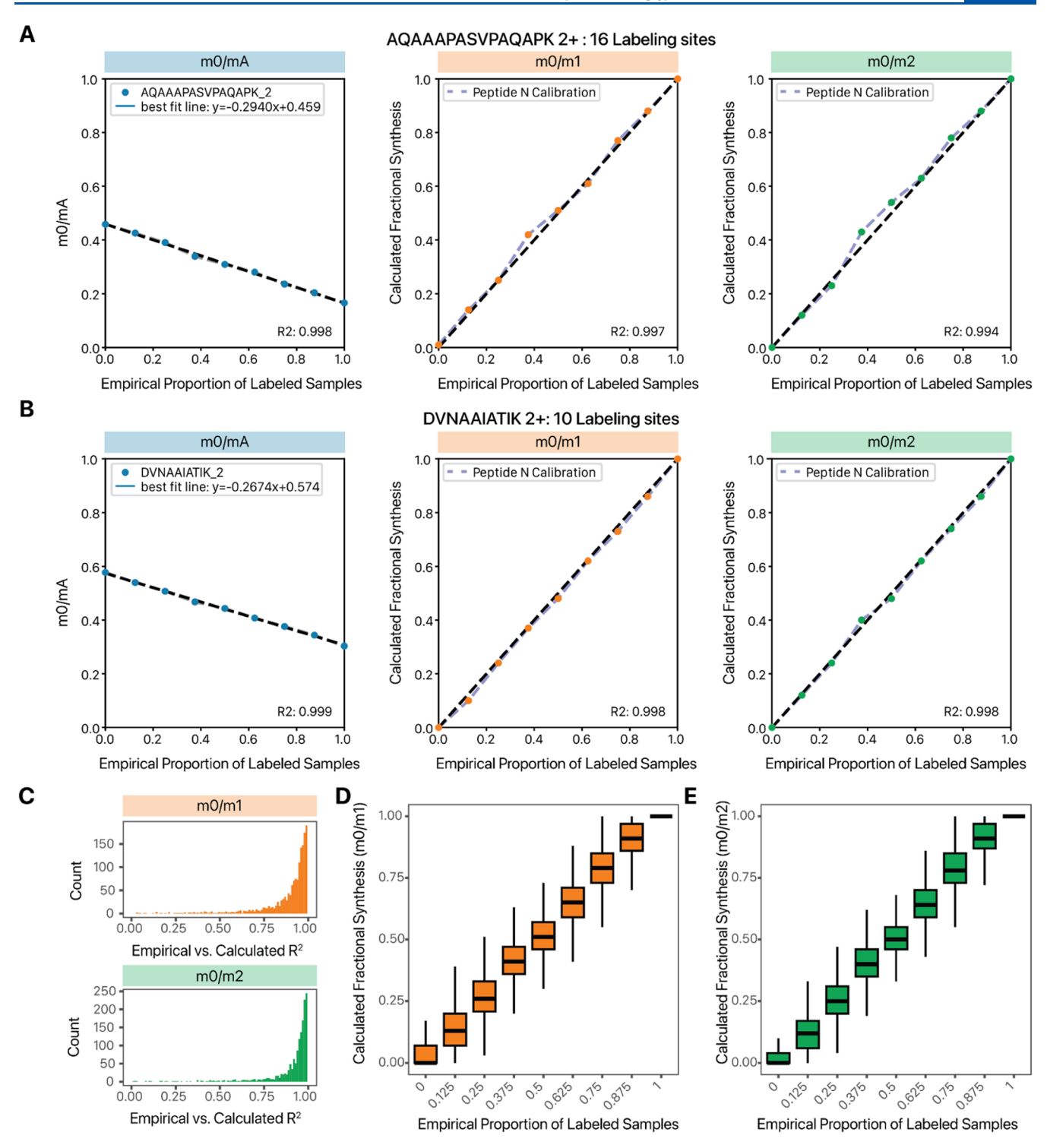


Figure 4. Mass isotopomer ratio calibration experiment using fully unlabeled and fully labeled samples. (A, B) Human AC16 cells were labeled fully through 9 doublings in 6% D<sub>2</sub>O, then mixed with unlabeled cells at a fixed proportion (0, 12.5, 25, 37.5, 50, 62.5%, 75, 87.5, and 100% of the labeled cells). Two exemplary peptides ((A) AQAAAPASVPAQAPK and (B) DVNAAIATIK) are shown with a linear decrease in the  $m_0/m_1$  ratio from 0 to 100% labeling experiment (left). Using the nearest-lookup method, we plotted the calculated  $\theta$  (y-axis) from empirical  $m_0/m_1$  (center) and  $m_0/m_2$  (right) against the known mixture proportion (x-axis). (C) Histogram of  $R^2$  values between empirical proportion of labeled samples vs calculated  $\theta$  from the  $m_0/m_1$  (top) and  $m_0/m_2$  (bottom) ratios. Among 1672 quantified peptide-charge pairs, 67.3% had  $R^2$  values  $\geq$  0.9 in the  $m_0/m_1$  ratio and 74.5% had  $R^2$  values  $\geq$  0.9 in the  $m_0/m_2$  ratios. Center lines: median; boxes: interquartile range; whiskers: 1.5× interquartile range.

reprocessed the experimental data from heavy water labeling experiments where proteins from the mouse heart were measured by mass spectrometry following up to  $\sim$ 4.6% total

body water deuterium enrichment in the animals at 12 time points for up to 31 days (Figure 3B).

This led to several observations. First, in the three peptides above, it can be seen that the nearest  $\theta$  lookup method returns  $\theta$ 

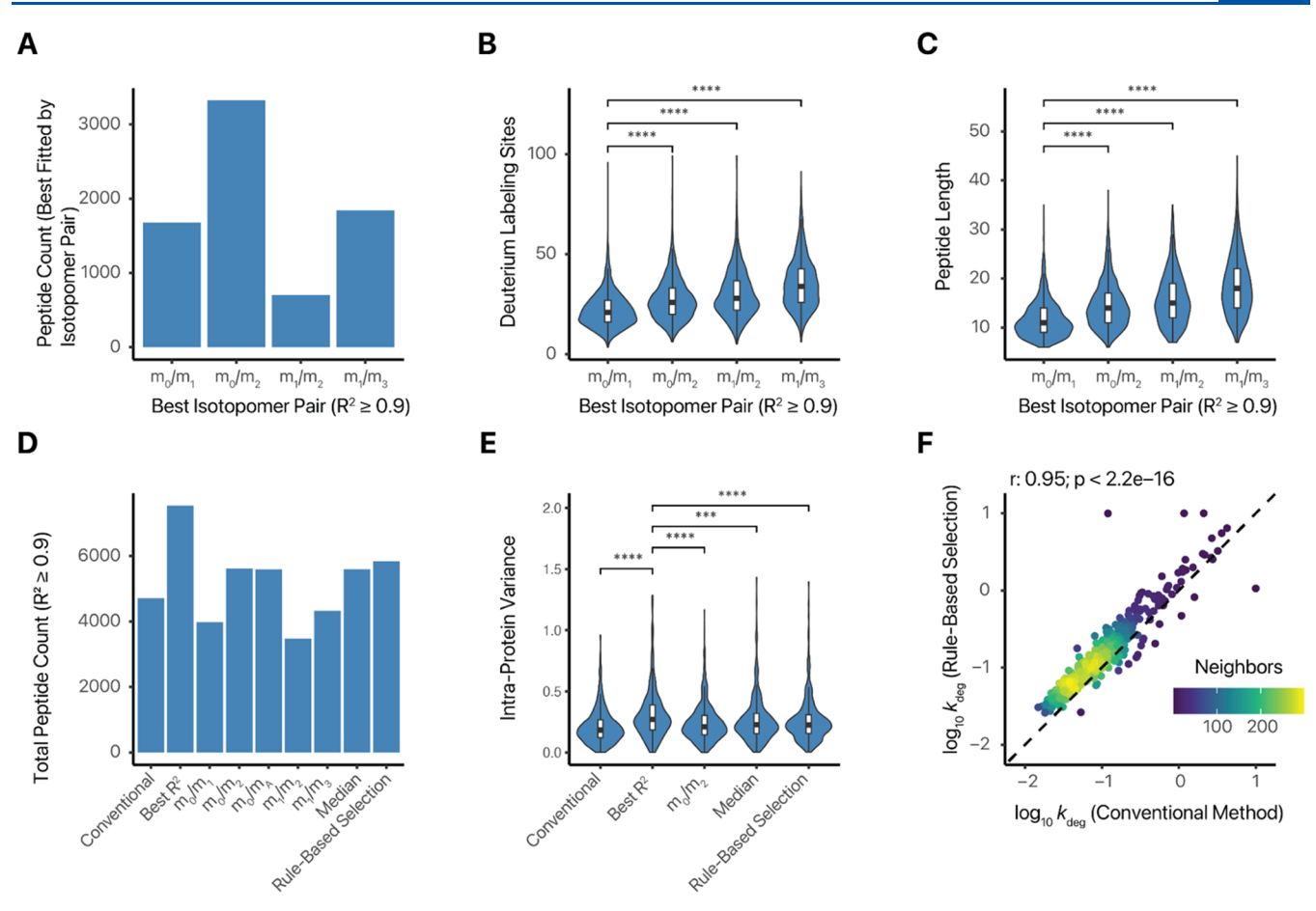


Figure 5. Comparison of number of quantifiable peptides at different  $R^2$  thresholds using different mass isotopomer pairs. (A) Bar charts showing the number of peptides (y-axis) across four categories, where a particular mass isotopomer ratio (x-axis) provides the best fit to the kinetic model over the other ratios. (B) Box plots showing the number of labeling sites in the peptides for which each of the mass isotopomer ratio provided the best-fit  $R^2$  (only  $R^2 \ge 0.9$  accepted) \*\*\*\*: Student's t test P < 2.2e-16. (C) Box plots showing the sequence lengths of peptides across each category. \*\*\*\*: Student's t test P < 2.2e-16. (D) Total number of well-fitted peptides ( $R^2 \ge 0.9$ ) in the Hammond et al. mouse heart data when using different  $\theta$  calculation methods ("Best  $R^2$ " refers to picking the best  $R^2$  out of four mass isotopomer pairs after curve fitting with each of them; <sup>14</sup> "Median" refers to taking the median values of  $\theta$  estimated by nearest lookup from all pairwise ratios of  $m_0$ ,  $m_1$ ,  $m_2$ , and  $m_3$ ). (E) Intraprotein variance, defined as the geometric coefficients of variance of  $k_{\text{deg}}$  of peptides mapping uniquely to the same protein, calculated from well-fitted peptides using different  $\theta$  calculation methods. \*\*\*\*Student's t test P < 2.2e-16. (F) Scatterplot showing the derived  $\log_{10} k_{\text{deg}}$  values in the "Rule-Based Selection" method over the values using the "Conventional" method as reported in the original study.

values that are consistent with one another and also consistent with the conventional method of calculation used in the original study (black dashed lines). This agreement appeared to be strongest for the short peptide with a few labeling sites. In the two longer peptides with more labeling sites, the  $m_0/m_1$  values deviate more from the other ratios. This is particularly apparent at later time points of labeling, where the  $\theta$  is higher. The conventional method of "complete" isotopic envelope therefore under-reports true  $\theta$  compared to the partial mass isotopomer profiles, which is consistent with appreciable m<sub>6</sub> and above peaks in the isotope envelope. Notably, this deviation from the conventional method  $\theta$  is observed in all of the mass isotopomer pair calculations with the isotopic calculator (i.e.,  $m_0/m_1$ ,  $m_0/m_2$ ,  $m_1/m_2$ ,  $m_1/m_3$ ,  $m_0/m_A$ , Figure 3B). When the full  $(\theta, t)$  series is used for curve fitting, the use of  $m_0/m_2$  and  $m_1/m_3$  marginally improved the curve-fitting  $R^2$  value, and also returned a higher calculated turnover rate for the peptide over the conventional method (Figure 3C). This analysis highlights that calculation of  $\theta$  from numerically resolved isotopic profiles is sufficient and may even improve kinetic modeling.

## Validation of Nearest $\theta$ Lookup Using a Heavy Water Labeling Calibration Standard

To verify that the limited mass isotopomer ratios returned numerically accurate  $\theta$  values, we first set up a calibration standard experiment, where cultured human cells are cultured in 6% deuterium oxide for at least 9 doublings, estimated to lead to >99.8% complete labeling of all protein pools to their plateau deuterium relative isotope abundance ratios, i.e., all protein species are ~100% labeled with 6% deuterium. This fully labeled pool is then mixed with nondeuterium-labeled cell lysate at the fixed proportions of 0, 12.5, 25, 37.5, 50, 62.5, 75, 87.5, and 100% to establish the ground truth of the simulation of  $\theta$  in each sample.

We focused on 1672 peptides (from 666 protein groups) that were reliably identified in all nine mixture proportion experiments and were well-behaved, as in having the proportion of  $m_0$  steadily decreasing in a linear fashion with increasing proportion of labels, with a linear fitting  $R^2$  of 0.9, suggesting the mass isotopomer profiles for these peptides are accurately measured by the mass spectrometer and quantified by the software tool (Figure 4A,B; Table S1). We then calculated the initial

(unlabeled) and final (fully labeled) full isotopic profiles using IsoSpec2, numerically looked up the value of  $\theta$  for the empirical mass isotopomer ratios using the mixed profiles as above, and compared the results with the ground truth mixture proportions. The resulting  $\theta$  curves largely maintained linearity and closely estimated the ground truth (two examples in Figure 4A,B) Overall, considering all 1672 peptides, the  $\theta$  lookup from  $m_0/m_1$  showed a strong linear relationship close to unity (y=0.9688x+0.041) and good agreement with the ground truth ratios ( $R^2$ : 0.888) (Figure 4C,D) as does the  $m_0/m_2$  ratio (y=0.9847x+0.024;  $R^2$ : 0.890) (Figure 4C,E). We conclude that the nearest isotopic profile lookup method returns reliable  $\theta$  values.

## Rule-Based Selection of Mass Isotopomer Ratio Based on Peptide Sequence Features

We next calculated the  $\theta$  profile toward the entire mouse heart data set for every distinct peptide-charge combination (hereafter "peptides"). To explore the potential effects of peptide abundance but minimize the bias of ambiguous protein assignment, we focused on peptides that are uniquely mapped to a single UniProt entry, have been quantified in 4 or more labeling time points to permit reliable curve fitting, and have nonzero integrated intensities in  $m_0$ ,  $m_1$ ,  $m_2$ , and  $m_3$  isotopomers. In total, we estimated  $\theta$  and performed curve fitting for 13,155 peptide time series. Using the conventional method, we derived the turnover rates of 4714 distinct peptides that fit well to the kinetic model with  $R^2 \ge 0.9$ . We then compared this performance to that of calculations based on partial mass isotopomer profiles. Through discrete curve fitting for each of the  $m_0/m_1$ ,  $m_0/m_2$ ,  $m_1/m_2$ ,  $m_0/m_3$ , isotopomer ratios, and picking the isotopomer that gives the best  $R^{2}$  value, we boosted the number of well-fitted peptides ( $R^2 \ge 0.9$ ) by 60% (7545 wellfitted peptides), which is comparable to the gain reported by Deberneh et al., 14 who selected the mass isotopomer ratio pair to use by first performing curve fitting on all quantified pairs, then choosing the one with the highest best-fit  $R^2$  value for each peptide. Although this "Best  $R^2$ " method leads to impressive gains, we reason that because the ratios derived from these mass isotopomer pairs would be expected to vary, the use of multiple  $\theta$ series to elect for the best fit is a case of multiple testing, where the  $R^2$  values are used first to compare the mass isotopomer pairs and select the best fit and then to report the final peptide goodness-of-fit. Moreover, this post hoc selection strategy does not allow a principled way to select the mass isotopomer ratio to use when only partial experimental data were collected or in experimental design, where it is only possible to collect samples from one labeling time point. We therefore wonder whether the fitting could be improved using a priori rules, without relying on a comparison of R<sup>2</sup> values after curve fitting. Contrary to the report by Debeneh et al., the mass isotopomer ratios had unequal contributions to fitting improvements, with  $m_0/m_2$ being the ratio that led to the best  $R^2$  in 44% of the peptides, followed by  $m_1/m_3$  (24%), then  $m_0/m_1$  (22%), and then  $m_1/m_2$ (9%) (Figure 5A), which we attribute to differential sensitivity of the mass isotopomer pairs to  $\theta$  in different peptides (Figure 2).

Notably, there is a strong relationship between the mass isotopomer ratios that lead to the best fit with the number of deuterium-accessible labeling sites  $n_l$  (Figure 5B) and implicitly, the sequence length (Figure 5C) of the peptides (Student's t test P < 2.2e-16). This may be because, for short and medium peptides, the  $m_0/m_2$  ratio spans the widest range of ratios across  $\theta$  (Figure 3A) and high peak intensity for accurate integration, both of which improve  $\theta$  calculation. On the other hand, for very

ı

long peptides with many labeling sites, the  $m_0$  isotopomer intensity has a very low relative abundance that renders it less effective in accurate  $\theta$  estimation (Figure 2A).

We therefore derived a simple mass isotopomer selection heuristics, where peptides with <15 labeling sites are quantified using  $m_0/m_1$ , peptides with 15  $\leq$  labeling sites  $\leq$ 35 are quantified with  $m_0/m_2$ , and peptides with >35 labeling sites are quantified with  $m_1/m_3$  isotopomer ratios. In the mouse heart data set, this "rule-based selection" approach modestly outperforms quantifying with  $m_0/m_2$  alone, and was able to improve on the conventional method by 24% (5842 vs 4714 peptides) without freely picking the best-fit  $R^2$  values from multiple mass isotopomer pairs for each peptide (Figure 5D). As an alternative method, we also took the median  $\theta$  calculated from all possible ratios between  $m_0$ ,  $m_1$ ,  $m_2$ , and  $m_3$  and found that in our hands it performs similarly to  $m_0/m_2$ . At the same time, the rule-based selection method was able to keep intraprotein variance under control, suggesting it returns internally consistent protein  $k_{\rm deg}$ values. We calculated intraprotein variance of a method as the median of median absolute deviation of  $k_{\text{deg}}$  values among peptides that compose a uniquely mapped protein with 3 or more peptides; the intraprotein variance of the rule-based selection method is similar to the conventional method (Figure 5E). On the other hand, post hoc selection of isotopomers (i.e., the "best R2" method) is associated with significantly higher intraprotein variance; in other words, the  $k_{\text{deg}}$  values of peptides within the protein are more different from each other. Given that the measured isotopomer ratios would be expected to vary, we speculate that picking mass isotopomer ratios for each peptide after curve fitting may increase the risk of overfitting but caution that additional work is needed to evaluate precision and accuracy in different data sets. Finally, the returned protein  $k_{\text{deg}}$ values are highly correlated between the conventional and rulebased selection methods (r: 0.95, P < 2.2e–16). There is a slight bias toward faster turnover in the rule-based selection method over the conventional method, as might be expected from the exclusion of higher mass isotopomers in the conventional method (Figure 5F). This bias is absent when comparing the rule-based selection method to the median  $\theta$  values of mass isotopomers (Figure S3). Overall, we surmise that the rule-based selection method did not introduce significant errors in the measured turnover rates.

To further investigate the factors that influence this gain in performance, we examined the differences in standard errors (s.e.) of fitting between mass isotopomer pairs and the conventional method and performed a linear regression analysis against several peptide parameters (Figure S2). Examining the performance gain (i.e., decrease in s.e.) of the  $m_1/m_3$ isotopomer pair, we find that the reduction in fitting s.e. is significantly and positively correlated with peptide length (linear model P: 5.3e-5), suggesting that fitting improvements are more pronounced among longer peptides (Figure S2A). On the other hand, when examining the  $m_0/m_1$  isotopomer pair, the reduction in s.e. correlates negatively with the peptide length, suggesting it particularly improves shorter peptides as expected (linear model P < 2.2e-16; Figure S2B). Upon combining  $m_0$ /  $m_1$ ,  $m_0/m_2$ , and  $m_1/m_3$  into the rule-based selection method, we find that peptides with shorter lengths continue to contribute more to fitting improvements; at the same time, there is a positive relationship between s.e. reduction with lower peptide label-free abundance, suggesting the rule-based selection method benefits low abundance peptides (Figure S2C). Finally, there is a positive correlation between the s.e. reduction with the

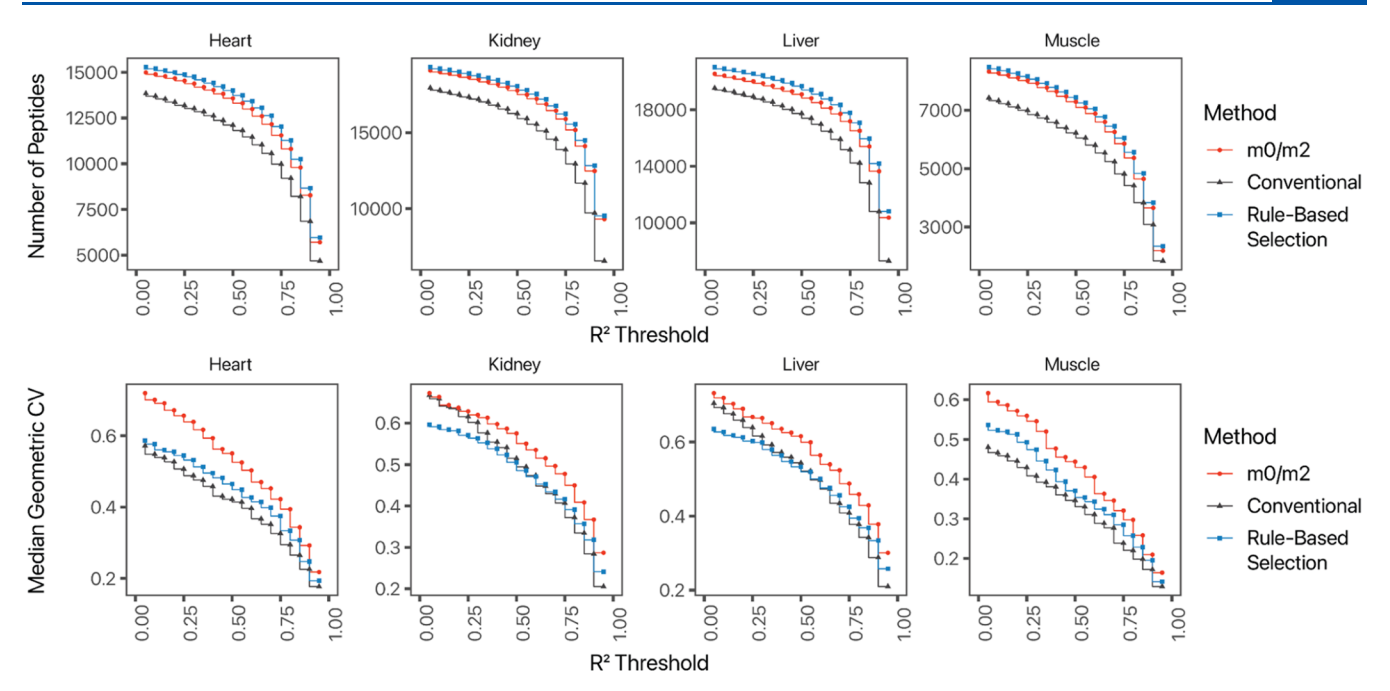


**Figure 6.** Increased depths of protein turnover measurements in four organs. Line plots showing the number of peptides (y) passing different  $R^2$  thresholds (top) and the resulting intraprotein variance (bottom) at each threshold across four experiments (heart, kidney, liver, and muscle) from Hammond et al., when calculated using three different methods: conventional  $m_0/m_A$  (gray),  $m_0/m_2$  (red), and rule-based selection (blue).

variance in the fraction of newly synthesized proteins when calculated from different mass isotopomer pairs (Figure S2D), suggesting the median fraction of all possible ratios might be useful for identifying the real fraction at each time point and that outlier removal methods may further improve  $\theta$  calculation. More generally, this result indicates that a combination of factors, including peptide labeling sites, measurement errors, and isobaric peptide interferences, likely play a role in explaining the improvements from the rule-based selection method.

## Implementation of the Rule-Based Mass Isotopomer Ratio Selection Strategy to Analyze Protein Turnover Rates from Multiple Data Sets

We implemented the rule-based mass isotopomer ratio selection method to the latest version of Riana, applying the Riana integration and curve-fitting workflow to the full set of mouse organ turnover experiments, which contain turnover information from two fast-turnover tissues (mouse liver and mouse kidney) and two slow-turnover tissues (mouse heart and skeletal muscle). In each of the tested experiments, we observed a consistent increase in the number of well-fitted peptides across multiple R<sup>2</sup> thresholds (Figure 6). Under a data depth filter for peptides quantified at ≥6 time points to match the original study, the rule-based selection method led to 27% (8666 vs 6851 peptides), 32% (12,830 vs 9707 peptides), 31% (14,190 vs 10,797 peptides), and 25% (3835 vs 3081 peptides) gain at  $R^2 \ge$ 0.9 for the heart, kidney, liver, and muscle data. At this  $R^2$  cutoff, the gain was greater for the liver and the kidney, which were high-turnover tissues and likely also had a less formidable dynamic range of concentration compared to the two muscle tissues with abundant muscle proteins. We saw a substantial increase in the depth of the turnover measurements in all four tissues than was published. In the liver, for instance, the selection method led to more proteins (1631 vs 1370) with well-fitted turnover rate information based on the same  $R^2 \ge 0.9$  threshold. These proteins include those with liver-based expression and function, such as cytochrome P450 monooxygenases 2C37

(CYP2C37) and 2C44 (CYP2C23), which are involved in polyunsaturated fatty acid metabolism, with measured turnover rates of 1.15 and 1.23/d ( $R^2$  0.961 and 0.903), respectively. Hence, the improved analysis can lead to more protein turnover information being recovered from existing data sets.

Finally, we further applied the combined rule-based selection method to two data sets generated independently by two groups, including a data set of C57BL/6J mouse liver 10 and a data set of mouse hearts of the A/J and BALB/c strains, with or without isoproterenol-induced cardiac hypertrophy. <sup>2,11</sup> The first data set was generated in an Orbitrap Eclipse instrument in FT/IT mode. The latter was generated in an Orbitrap Elite instrument in FT/IT mode, with substantial fractionation consisting of biological subcellular fractionations into the cytosolic, mitochondrial, and nuclear enriched fractions, followed by twodimensional peptide fractionation. The use of rule-based mass isotopomer ratio selection and nearest-lookup of  $\theta$  again led to substantial increase in the coverage of well-fitted  $(R^2 \ge 0.9)$ ; identified at  $\geq 4$  time points as in the original study) peptides by  $58\% \pm 13\%$  (s.d.), while keeping intraprotein variance under control to be generally below 25% (Table 2). A similar increase is observed when curve-fitting  $R^2$  cutoffs of 0.7 and 0.8 are used (Figure S4). The improved coverage also led to an increase in the number of protein groups whose turnover rates are commonly quantified in both control and hypertrophy mouse hearts (e.g., 2702 vs 2427 proteins in A/J mice); hence the presented method may facilitate comparative studies to find proteins with differential turnover in aging or disease.

#### DISCUSSION

Our group and others have applied heavy water labeling to examine the regulation of protein turnover in various adult animals and disease models. 1,4,8,11 Compared to more commonly employed dynamic SILAC experiments, heavy water labeling has the advantages of quick precursor equilibration, low cost, bioorthogonality, and being applicable

Table 2. Increasing the Depth of Protein Turnover Coverage in 13 Additional Sets of Turnover Time Series Data from 3 Mouse Strains across 2 Studies<sup>a</sup>

			conventional			rule-based mass isotopomer ratio selection (this study)				
animal	organ/subcellular enriched fraction	proteome Xchange accession	num. peptides $(R^2 \ge 0.9)$	num. protein groups	variance (%)	num. peptides $(R^2 \ge 0.9)$	num. protein groups	variance (%)	gain in coverage (%)	
A/J control	heart cytosolic	PXD002870	2931	1351	18.3	4679	1741	21.4	60	
A/J control	heart mitochondrial	PXD002870	1302	654	19.7	2336	932	21.6	79	
A/J control	heart nuclear/ insoluble	PXD002870	3002	957	24.8	4755	1241	28.9	58	
A/J hypertrophy	heart cytosolic	PXD002870	4173	1728	22.3	6636	2183	23.8	59	
A/J hypertrophy	heart mitochondrial	PXD002870	1508	722	19.5	2749	1007	21.4	82	
A/J hypertrophy	heart nuclear/ insoluble	PXD002870	2438	732	21.1	4034	1021	24.9	65	
BALB/c control	heart cytosolic	PXD002870	2792	1317	18.2	3894	1598	21.0	39	
BALB/c control	heart mitochondrial	PXD002870	2641	1035	20.4	3667	1316	20.9	39	
BALB/c control	heart nuclear/ insoluble	PXD002870	1774	742	19.8	2765	970	21.5	56	
BALB/c hypertrophy	heart cytosolic	PXD002870	3379	1460	19.6	4882	1808	22.2	44	
BALB/c hypertrophy	heart mitochondrial	PXD002870	1466	759	18.3	2459	1025	21.1	68	
BALB/c hypertrophy	heart nuclear/ insoluble	PXD002870	1284	477	18.0	1961	622	19.2	53	
C57BL/6J	liver total	PXD036140	5318	1529	18.6	8542	2098	22.3	61	

<sup>&</sup>quot;Peptides quantified at more than half of the time points in each study were admitted for curve fitting. Variance is calculated as the median of the geometric CV of proteins with 3 or more unique peptides fitted to the kinetic model at  $R^2 \ge 0.9$ .

to many different types of tissues and animals. However, wider applications continue to be hurdled by the relative complexity in the interpretation of spectral data to extract the fraction of newly synthesized proteins at each sampled time point. A heavy water labeled peptide can be considered as a polymer of multiple deuterium-accessible labeling sites, and the isotopic profile is a summation across the combinatorial possibilities of site labeling, factoring in the number of deuterium-accessible labeling sites, and the probability of incorporation of a deuterium atom (which is related, in turn to the precursor water enrichment). Mass isotopomer distribution analysis shows that each isotopomer contains information regarding the relative isotope enrichment and molar fraction of synthesized peptides. Recent work, notably by Sadygov and colleagues, showed that "limited isotopomers", i.e., using ratios of specific subsets of isotopically labeled ions rather than the full isotopic envelope, can be applied to heavy water labeling. 18 Here, we build on these prior works in three ways, by reporting (1) a straightforward "nearest-lookup" method to find the molar fraction of new synthesis from numerically approximated peptide isotopic profiles in heavy water labeling studies; (2) a "rule-based mass isotopomer ratio selection" method that selects the mass isotopomer to use for  $\theta$ calculation based on total deuterium-accessible labeling sites in a peptide; and (3) implementation of the combined methods in Riana, an open-source software suited for analyzing mass spectrometry data from multiple stable isotope labeling experimental designs.

Numerical calculation of partial mass isotopomer profiles using isotopic fine structure algorithms allows different mass isotopomer ratios from empirical spectra to be matched to the simulated composite spectra to find the fraction of new syntheses in heavy water labeled peptides. Here, we provide corroborating evidence that the use of mass isotopomer pairs is

sufficient for  $\theta$  calculation and improves upon the conventional "complete" isotopic profile method. Moreover, we find that the  $m_0/m_2$  ratio increases goodness-of-fit  $(R^2)$  to the kinetic model in the greatest number of peptides, but does not perform as well for long peptides or peptides with great numbers of deuteriumaccessible labeling sites. We derived a simple heuristic mass isotopomer selection strategy where peptides with the number of accessible labeling sites  $n_1$  < 15 are quantified with  $m_0/m_1$ , 15  $\leq n_1 \leq 35$  with  $m_0/m_2$ , and  $n_1 > 35$  peptides are quantified with  $m_1/m_3$ . We show that this simple selection strategy based on a priori defined rules is able to boost the number of peptides with well-fitted mass isotopomer trajectory over time to the kinetic model  $(R^2 \ge 0.9)$  substantially. Interestingly, we find that the approach of looking up the nearest simulated  $\theta$  in the calculated isotopologue profiles already improves upon the conventional method of the monoisotopomer relative abundance calculation, even when identical mass isotopomers (i.e.,  $m_0/\sum (m_0:m_5)$ ) are used (Figure 5D). This suggests that other factors may also contribute to the improved turnover profiling coverage beyond the reduction of isobaric contaminant peptides.

These factors may include, first, the composite lookup method (eq 6) being bounded to  $0 \le \theta \le 1$ , whereas the conventional calculation (eq 5) is not and can return negative  $\theta$  values unless additional boundary conditions are set. This can happen for instance when the proportion of the monoisotopomer in the complete envelope is lower than prelabeling naturally occurring values or higher than the theoretical asymptotic probability due to measurement errors. Second, for longer peptides, the use of the first six mass isotopomers in the conventional calculation would underestimate  $\theta$  because the  $m_6-m_8$  peaks have appreciable intensity, and hence  $m_0/m_A$  loses linearity over  $\theta$ . This is not the case in the lookup method because the contributions of  $m_6+$  peaks are accounted for in

both the empirical values and the composite simulated spectra. Third, as noted above, different mass isotopomer ratios span different ranges and hence would offer differential sensitivity in quantification, whereas for longer peptides, the mo peaks are diminutive even prior to labeling and may not lend to accurate measurements. Taken together, we propose that a combination of factors likely contribute to the advantages of partial mass isotopomer profiles whether calculated from closed-form equations or from isotopic fine structure algorithms. Indeed, different mass isotopomers appear to best support goodness-offit to kinetic models for peptides with differential molecular weights or numbers of deuterium labeling sites. Overall, the combined nearest-lookup and rule-based mass isotopomer ratio selection method improved on conventional methods by up to an average of 58% when we reanalyzed multiple existing D2O labeling experiments from different groups. This strategy is implemented in Riana, an open-source Python software for protein turnover quantification compatible with heavy water and amino acid labeling.

#### **■ LIMITATIONS OF THE STUDY**

Although numerical estimation presents a convenient calculation of the fraction of newly synthesized proteins/peptides from mass isotopomer ratios, it is worth noting that closed-form solutions of mass isotopomer ratios<sup>14</sup> have the advantages of modeling the distributions of deuterium atoms on individual peptide molecules and allowing model sensitivity analysis.

Second, the number of deuterium sites per peptide is a major variable in the analysis of heavy water labeling data. The calibration standards are performed with labeled human AC16 cells in culture, which are expected to incorporate fewer deuterium atoms per amino acid than in animal models.<sup>27,28</sup> In other words, the peptide sequences, if identified in animal tissue samples, would be expected to incorporate more deuterium atoms. We note that this difference does not prevent the use of the calibration standards in this study because the peptide labeling sites in the standards are calculated from the plateau enrichment values directly and are not contingent upon knowing individual amino acid labeling sites, which allows their use for comparing  $\theta$  calculation methods. However, a "gold standard" fully labeled animal tissue with a majority of peptides having greater numbers of exchangeable sites remains to be established and will likely prove to be useful for continued method development.

Lastly, the contributions of different parameters to the gain in coverage, such as the instrument type and AGC, remain to be established. Further analysis is needed to optimize strategies for determining which peptide measurements may yield suitable turnover information prior to curve fitting. These limitations suggest possible areas for future development.

#### ASSOCIATED CONTENT

#### **Data Availability Statement**

Source data of calibration standard are available in Table S1. Riana is open-source and freely available on GitHub at http://github.com/ed-lau/riana. A visualization web app for mass isotopomer envelopment is available at http://heart.shinyapps.io/D2O\_Isotope/. The reanalyzed data sets are available on ProteomeXchange at PXD029639, PXD002870, and PXD036140. The AC16 calibration standard mass spectrometry data generated as part of this study are available on ProteomeXchange at PXD048321.

#### **Supporting Information**

The Supporting Information is available free of charge at https://pubs.acs.org/doi/10.1021/acs.jproteome.4c01012.

Additional simulated isotope envelopes in heavy water labeled samples (Figure S1); parameters associated with improved turnover quantifications from partial mass isotopomer profiles (Figure S2); comparison of "Rule-Based Selection" vs "Median" methods (Figure S3); and increased number of confidently quantified peptides in fractionated protein turnover data sets (Figure S4) (PDF) Mass isotopomer ratios at different true proportion mixtures of unlabeled and fully labeled proteins in the calibration standard experiment (Table S1) (XLSX)

#### AUTHOR INFORMATION

#### **Corresponding Authors**

Maggie P. Y. Lam — Department of Medicine, University of Colorado School of Medicine, Aurora, Colorado 80045, United States; Consortium for Fibrosis Research and Translation and Department of Biochemistry and Molecular Genetics, University of Colorado School of Medicine, Aurora, Colorado 80045, United States; Email: maggie.lam@cuanschutz.edu

Edward Lau — Department of Medicine, University of Colorado School of Medicine, Aurora, Colorado 80045, United States; Consortium for Fibrosis Research and Translation, University of Colorado School of Medicine, Aurora, Colorado 80045, United States; orcid.org/0000-0001-9083-5922; Email: edward.lau@cuanschutz.edu

#### **Authors**

Jordan Currie — Department of Medicine, University of Colorado School of Medicine, Aurora, Colorado 80045, United States; Consortium for Fibrosis Research and Translation, University of Colorado School of Medicine, Aurora, Colorado 80045, United States

Dominic C. M. Ng — Department of Medicine, University of Colorado School of Medicine, Aurora, Colorado 80045, United States; Consortium for Fibrosis Research and Translation, University of Colorado School of Medicine, Aurora, Colorado 80045, United States

Boomathi Pandi — Department of Medicine, University of Colorado School of Medicine, Aurora, Colorado 80045, United States; Consortium for Fibrosis Research and Translation, University of Colorado School of Medicine, Aurora, Colorado 80045, United States

Alexander Black — Department of Medicine, University of Colorado School of Medicine, Aurora, Colorado 80045, United States; Consortium for Fibrosis Research and Translation, University of Colorado School of Medicine, Aurora, Colorado 80045, United States

Vyshnavi Manda – Department of Medicine, University of Colorado School of Medicine, Aurora, Colorado 80045, United States; Consortium for Fibrosis Research and Translation, University of Colorado School of Medicine, Aurora, Colorado 80045, United States

Cheyanne Durham – Department of Medicine, University of Colorado School of Medicine, Aurora, Colorado 80045, United States; Consortium for Fibrosis Research and Translation, University of Colorado School of Medicine, Aurora, Colorado 80045, United States

Jay Pavelka – Department of Medicine, University of Colorado School of Medicine, Aurora, Colorado 80045, United States; Consortium for Fibrosis Research and Translation, University of Colorado School of Medicine, Aurora, Colorado 80045, United States

Complete contact information is available at: https://pubs.acs.org/10.1021/acs.jproteome.4c01012

#### **Author Contributions**

J.C. and D.C.M.N. contributed equally.

Notes

The authors declare no competing financial interest.

#### ACKNOWLEDGMENTS

The authors thank Prof. Robert J Beynon at the University of Liverpool for helpful discussions and editing of the manuscript. This work was supported in part by NIH Awards R35-GM146815 and R01HL169473; the University of Colorado SOM Translational Scholar Research Program to E.L.; and NIH awards R01HL169473, R01HL141278, and R01GM144456 to M.L.

#### REFERENCES

- (1) Shekar, K. C.; Li, L.; Dabkowski, E. R.; Xu, W.; Ribeiro, R. F.; Hecker, P. A.; Recchia, F. A.; Sadygov, R. G.; Willard, B.; Kasumov, T.; Stanley, W. C. Cardiac Mitochondrial Proteome Dynamics with Heavy Water Reveals Stable Rate of Mitochondrial Protein Synthesis in Heart Failure despite Decline in Mitochondrial Oxidative Capacity. *J. Mol. Cell. Cardiol.* **2014**, *75*, 88–97.
- (2) Lau, E.; Cao, Q.; Ng, D. C. M.; Bleakley, B. J.; Dincer, T. U.; Bot, B. M.; Wang, D.; Liem, D. A.; Lam, M. P. Y.; Ge, J.; Ping, P. A Large Dataset of Protein Dynamics in the Mammalian Heart Proteome. *Sci. Data* **2016**, *3*, No. 160015.
- (3) Kim, T.-Y.; Wang, D.; Kim, A. K.; Lau, E.; Lin, A. J.; Liem, D. A.; Zhang, J.; Zong, N. C.; Lam, M. P. Y.; Ping, P. Metabolic Labeling Reveals Proteome Dynamics of Mouse Mitochondria. *Mol. Cell. Proteomics* **2012**, *11* (12), 1586–1594.
- (4) Price, J. C.; Khambatta, C. F.; Li, K. W.; Bruss, M. D.; Shankaran, M.; Dalidd, M.; Floreani, N. A.; Roberts, L. S.; Turner, S. M.; Holmes, W. E.; Hellerstein, M. K. The Effect of Long Term Calorie Restriction on in Vivo Hepatic Proteostatis: A Novel Combination of Dynamic and Quantitative Proteomics. *Mol. Cell. Proteomics* **2012**, *11* (12), 1801–1814.
- (5) Busch, R.; Kim, Y.; Neese, R.; Schadeserin, V.; Collins, M.; Awada, M.; Gardner, J.; Beysen, C.; Marino, M.; Misell, L. Measurement of Protein Turnover Rates by Heavy Water Labeling of Nonessential Amino Acids. *Biochim. Biophys. Acta, Gen. Subj.* **2006**, *1760* (5), 730–744.
- (6) Hammond, D. E.; Simpson, D. M.; Franco, C.; Wright Muelas, M.; Waters, J.; Ludwig, R. W.; Prescott, M. C.; Hurst, J. L.; Beynon, R. J.; Lau, E. Harmonizing Labeling and Analytical Strategies to Obtain Protein Turnover Rates in Intact Adult Animals. *Mol. Cell. Proteomics* 2022, 21 (7), No. 100252.
- (7) Miller, B. F.; Reid, J. J.; Price, J. C.; Lin, H.-J. L.; Atherton, P. J.; Smith, K. CORP: The Use of Deuterated Water for the Measurement of Protein Synthesis. *J. Appl. Physiol.* **2020**, *128* (5), 1163–1176.
- (8) Lam, M. P. Y.; Wang, D.; Lau, E.; Liem, D. A.; Kim, A. K.; Ng, D. C. M.; Liang, X.; Bleakley, B. J.; Liu, C.; Tabaraki, J. D.; Cadeiras, M.; Wang, Y.; Deng, M. C.; Ping, P. Protein Kinetic Signatures of the Remodeling Heart Following Isoproterenol Stimulation. *J. Clin. Invest.* 2014, 124 (4), 1734–1744.
- (9) Price, J. C.; Holmes, W. E.; Li, K. W.; Floreani, N. A.; Neese, R. A.; Turner, S. M.; Hellerstein, M. K. Measurement of Human Plasma Proteome Dynamics with (2)H(2)O and Liquid Chromatography Tandem Mass Spectrometry. *Anal. Biochem.* **2012**, *420* (1), 73–83.
- (10) Deberneh, H. M.; Abdelrahman, D. R.; Verma, S. K.; Linares, J. J.; Murton, A. J.; Russell, W. K.; Kuyumcu-Martinez, M. N.; Miller, B. F.; Sadygov, R. G. A Large-Scale LC-MS Dataset of Murine Liver

- Proteome from Time Course of Heavy Water Metabolic Labeling. *Sci. Data* **2023**, *10* (1), No. 635.
- (11) Lau, E.; Cao, Q.; Lam, M. P. Y.; Wang, J.; Ng, D. C. M.; Bleakley, B. J.; Lee, J. M.; Liem, D. A.; Wang, D.; Hermjakob, H.; Ping, P. Integrated Omics Dissection of Proteome Dynamics during Cardiac Remodeling. *Nat. Commun.* **2018**, *9* (1), No. 120.
- (12) Shankaran, M.; King, C. L.; Angel, T. E.; Holmes, W. E.; Li, K. W.; Colangelo, M.; Price, J. C.; Turner, S. M.; Bell, C.; Hamilton, K. L.; Miller, B. F.; Hellerstein, M. K. Circulating Protein Synthesis Rates Reveal Skeletal Muscle Proteome Dynamics. *J. Clin. Invest.* **2016**, *126* (1), 288–302.
- (13) Fanara, P.; Wong, P.-Y. A.; Husted, K. H.; Liu, S.; Liu, V. M.; Kohlstaedt, L. A.; Riiff, T.; Protasio, J. C.; Boban, D.; Killion, S.; Killian, M.; Epling, L.; Sinclair, E.; Peterson, J.; Price, R. W.; Cabin, D. E.; Nussbaum, R. L.; Brühmann, J.; Brandt, R.; Christine, C. W.; Aminoff, M. J.; Hellerstein, M. K. Cerebrospinal Fluid—Based Kinetic Biomarkers of Axonal Transport in Monitoring Neurodegeneration. *J. Clin. Invest.* 2012, 122 (9), 3159—3169.
- (14) Deberneh, H. M.; Abdelrahman, D. R.; Verma, S. K.; Linares, J. J.; Murton, A. J.; Russell, W. K.; Kuyumcu-Martinez, M. N.; Miller, B. F.; Sadygov, R. G. Quantifying Label Enrichment from Two Mass Isotopomers Increases Proteome Coverage for in Vivo Protein Turnover Using Heavy Water Metabolic Labeling. *Commun. Chem.* 2023, 6 (1), No. 72.
- (15) Łącki, M. K.; Valkenborg, D.; Startek, M. P. IsoSpec2: Ultrafast Fine Structure Calculator. *Anal. Chem.* **2020**, *92* (14), 9472–9475.
- (16) Loos, M.; Gerber, C.; Corona, F.; Hollender, J.; Singer, H. Accelerated Isotope Fine Structure Calculation Using Pruned Transition Trees. *Anal. Chem.* **2015**, *87* (11), 5738–5744.
- (17) Dostal, V.; Wood, S. D.; Thomas, C. T.; Han, Y.; Lau, E.; Lam, M. P. Y. Proteomic Signatures of Acute Oxidative Stress Response to Paraquat in the Mouse Heart. *Sci. Rep.* **2020**, *10* (1), No. 18440.
- (18) Sadygov, R. G. Partial Isotope Profiles Are Sufficient for Protein Turnover Analysis Using Closed-Form Equations of Mass Isotopomer Dynamics. *Anal. Chem.* **2020**, 92 (21), 14747–14753.
- (19) Commerford, S. L.; Carsten, A. L.; Cronkite, E. P. The Distribution of Tritium among the Amino Acids of Proteins Obtained from Mice Exposed to Tritiated Water. *Radiat. Res.* **1983**, *94* (1), 151–155.
- (20) The UniProt Consortium; Bateman, A.; Martin, M.-J.; Orchard, S.; Magrane, M.; Ahmad, S.; Alpi, E.; Bowler-Barnett, E. H.; Britto, R.; Bye-A-Jee, H.; Cukura, A.; Denny, P.; Dogan, T.; Ebenezer, T.; Fan, J.; Garmiri, P.; Da Costa Gonzales, L. J.; Hatton-Ellis, E.; Hussein, A.; Ignatchenko, A.; Insana, G.; Ishtiaq, R.; Joshi, V.; Jyothi, D.; Kandasaamy, S.; Lock, A.; Luciani, A.; Lugaric, M.; Luo, J.; Lussi, Y.; MacDougall, A.; Madeira, F.; Mahmoudy, M.; Mishra, A.; Moulang, K.; Nightingale, A.; Pundir, S.; Qi, G.; Raj, S.; Raposo, P.; Rice, D. L.; Saidi, R.; Santos, R.; Speretta, E.; Stephenson, J.; Totoo, P.; Turner, E.; Tyagi, N.; Vasudev, P.; Warner, K.; Watkins, X.; Zaru, R.; Zellner, H.; Bridge, A. J.; Aimo, L.; Argoud-Puy, G.; Auchincloss, A. H.; Axelsen, K. B.; Bansal, P.; Baratin, D.; Batista Neto, T. M.; Blatter, M.-C.; Bolleman, J. T.; Boutet, E.; Breuza, L.; Gil, B. C.; Casals-Casas, C.; Echioukh, K. C.; Coudert, E.; Cuche, B.; De Castro, E.; Estreicher, A.; Famiglietti, M. L.; Feuermann, M.; Gasteiger, E.; Gaudet, P.; Gehant, S.; Gerritsen, V.; Gos, A.; Gruaz, N.; Hulo, C.; Hyka-Nouspikel, N.; Jungo, F.; Kerhornou, A.; Le Mercier, P.; Lieberherr, D.; Masson, P.; Morgat, A.; Muthukrishnan, V.; Paesano, S.; Pedruzzi, I.; Pilbout, S.; Pourcel, L.; Poux, S.; Pozzato, M.; Pruess, M.; Redaschi, N.; Rivoire, C.; Sigrist, C. J. A.; Sonesson, K.; Sundaram, S.; Wu, C. H.; Arighi, C. N.; Arminski, L.; Chen, C.; Chen, Y.; Huang, H.; Laiho, K.; McGarvey, P.; Natale, D. A.; Ross, K.; Vinayaka, C. R.; Wang, Q.; Wang, Y.; Zhang, J. UniProt: The Universal Protein Knowledgebase in 2023. Nucleic Acids Res. 2023, 51 (D1), D523-D531.
- (21) da Veiga Leprevost, F.; Haynes, S. E.; Avtonomov, D. M.; Chang, H.-Y.; Shanmugam, A. K.; Mellacheruvu, D.; Kong, A. T.; Nesvizhskii, A. I. Philosopher: A Versatile Toolkit for Shotgun Proteomics Data Analysis. *Nat. Methods* **2020**, *17* (9), 869–870.

- (22) Eng, J. K.; Hoopmann, M. R.; Jahan, T. A.; Egertson, J. D.; Noble, W. S.; MacCoss, M. J. A Deeper Look into Comet–Implementation and Features. *J. Am. Soc. Mass Spectrom.* **2015**, 26 (11), 1865–1874.
- (23) The, M.; MacCoss, M. J.; Noble, W. S.; Käll, L. Fast and Accurate Protein False Discovery Rates on Large-Scale Proteomics Data Sets with Percolator 3.0. *J. Am. Soc. Mass Spectrom.* **2016**, 27 (11), 1719–1727
- (24) Guan, S.; Price, J. C.; Ghaemmaghami, S.; Prusiner, S. B.; Burlingame, A. L. Compartment Modeling for Mammalian Protein Turnover Studies by Stable Isotope Metabolic Labeling. *Anal. Chem.* **2012**, *84* (9), 4014–4021.
- (25) Naylor, B. C.; Porter, M. T.; Wilson, E.; Herring, A.; Lofthouse, S.; Hannemann, A.; Piccolo, S. R.; Rockwood, A. L.; Price, J. C. DeuteRater: A Tool for Quantifying Peptide Isotope Precision and Kinetic Proteomics. *Bioinformatics* **2017**, 33 (10), 1514–1520.
- (26) Hellerstein, M. K.; Neese, R. A. Mass Isotopomer Distribution Analysis at Eight Years: Theoretical, Analytic, and Experimental Considerations. *Am. J. Physiol.: Endocrinol. Metab.* **1999**, 276 (6), E1146–E1170.
- (27) Busch, R.; Kim, Y.-K.; Neese, R. A.; Schade-Serin, V.; Collins, M.; Awada, M.; Gardner, J. L.; Beysen, C.; Marino, M. E.; Misell, L. M.; Hellerstein, M. K. Measurement of Protein Turnover Rates by Heavy Water Labeling of Nonessential Amino Acids. *Biochim. Biophys. Acta, Gen. Subj.* 2006, 1760 (5), 730–744.
- (28) Alamillo, L.; Ng, D. C. M.; Currie, J.; Black, A.; Pandi, B.; Manda, V.; Pavelka, J.; Schaal, P.; Travers, J. G.; McKinsey, T. A.; Lam, M. P. Y.; Lau, E. Deuterium Labeling Enables Proteome Wide Turnover Kinetics Analysis in Cell Culture. January 31, bioRxiv 2025 DOI: 10.1101/2025.01.30.635596.